Methods for Measuring and Representing Automobile Occupant Posture

Matthew P. Reed, Miriam A. Manary and Lawrence W. Schneider
University of Michigan Transportation Research Institute

GLOBAL MOBILITY DATABASE

All SAE papers, standards, and selected books are abstracted and indexed in the Global Mobility Database

Printed in USA

Methods for Measuring and Representing Automobile Occupant Posture

Matthew P. Reed, Miriam A. Manary and Lawrence W. Schneider
University of Michigan Transportation Research Institute

ABSTRACT

Many vehicle design and safety assessment applications use physical and virtual representations of vehicle occupants within the vehicle interior. Proper use of these human models requires accurate data concerning vehicle occupant posture and position. This paper presents techniques for characterizing vehicle occupant posture by measuring accessible body landmarks. The landmark locations are used to estimate joint locations that define a kinematic linkage representation of the human body. The resulting posture analysis techniques provide a unified method of measuring and reporting vehicle occupant postures that is suitable for use with both physical and virtual human models.

INTRODUCTION

The human body is commonly represented in ergonomic and biomechanical investigations as an open chain of rigid segments. The number of segments and the nature of the joints between segments varies widely depending on the application of the resulting kinematic model. A classic representation of the body for design purposes by Dempster (1)[1] divided the body into 13 planar segments, including a single segment from the hips to the top of the head. A contrasting model is presented by Nussbaum and Chaffin (2) who used multiple rigid, three-dimensional segments to simulate torso kinematics. There are many other whole- and partial-body models in the literature, with a wide range of complexity.

For automotive applications, two kinematic representations of the body have been most widely used. The Society of Automotive Engineers (SAE) J826 H-point manikin (3) provides four articulating segments (foot, leg, thigh/buttocks, and torso) to represent a vehicle occupant's posture. A two-dimensional template with similar contours is used with sideview design drawings. The joints of the H-point manikin and the two-dimensional template have a single degree of freedom, pivoting in a sagittal plane. These two tools are the standard occupant representations of vehicle interior design (4).

The other widely used kinematic representation of vehicle occupants is that embodied in the Anthropomorphic Test Devices (ATDs), or crash dummies, used to assess impact protection. The current standard ATD, the Hybrid-III, has many more degrees of freedom and body segments than the SAE H-point manikin or two-dimensional template, including three degrees of freedom at each hip, shoulder, and ankle (5). The lumbar and cervical spine are represented by flexible structures that allow flexion or extension in any plane. In a more recent development, Schneider et al. (6) presented new anthropometric data for an advanced family of crash dummies that were subsequently used in the development of a new ATD thorax that adds additional complexity to the shoulders, thoracic spine, and ribcage to obtain a more realistic interaction with restraint systems (7).

Software representations of both the SAE J826 and ATD linkages are now widely used in the vehicle design process. The design tools are intended for kinematic analysis only, but models of the ATDs are intended for dynamic use, i.e., crash simulation. In both vehicle ergonomics and impact protection, commercial human body representations are now available that provide models with additional complexity (8-10). The JOHN model, a three-dimensional kinematic tool intended for use in auto seat design, uses a six-joint lumbar spine to provide complex spine motions linked to changes in external contour (11). Bush (12) developed a two-dimensional seat design template with similar kinematics using a fixed motion distribution between two lumbar joints.

The objectives of the current work are:

1. to develop a kinematic representation of vehicle occupant posture for vehicle interior ergonomics applications relating to normal riding and driving postures while providing continuity with existing occupant protection tools, and

2. to develop techniques for measuring and representing posture using the kinematic model.

---

1. Numbers in parentheses denote references at the end of this paper.

This work is primarily a review and synthesis of previous studies. The emphasis here is on the efficient representation of vehicle occupant posture, using the smallest amount of information necessary to describe the posture to a level of detail sufficient for vehicle ergonomic applications relating to normal riding and driving postures.

It is useful to define "normal driving posture" as sagittally symmetric, with the sagittal plane aligned with the vehicle or seat sideview (XZ) plane. A large body of experimental data in vehicles and laboratory vehicle mockups has demonstrated that drivers, when instructed to sit with a "normal, comfortable driving posture," choose a torso posture that largely conforms to this definition. Asymmetric limb postures are resolved by recording the posture of only the right side of the body, since the right foot interaction with the accelerator pedal ensures that the right-leg posture is related to the driver's adaptation to the workspace. The techniques presented here are readily applied to either or both legs or arms, so that the sagittal symmetry requirement for the limbs can be relaxed if desired. By accepting this somewhat restrictive definition of normal driving (or riding) posture, the resulting kinematic constraints can be exploited to reduce the amount of body position information that is necessary to describe the posture.

As noted above, one of the objectives of the current work is to provide continuity between ergonomic applications and impact protection. This process has been facilitated by extensive use of the data and analysis on which the new family of frontal crash dummies is based. Robbins (13, 14) used three-dimensional surface landmark data from seventy-five drivers in three size categories to estimate the locations of anatomical joints that define a kinematic linkage. In the current analysis, ambiguities among various sources relating to joint locations have been resolved in favor of consistency with Robbins' analysis, except where the preponderance of evidence suggests that an alternative approach will significantly improve the location estimate.

Unfortunately, there is much less publicly available data for determining the relationship between surface anatomical landmarks and interior skeletal geometry than one might expect, given the importance of these calculations for so many ergonomic and biomechanical studies. The landmark studies in this area include Dempster (1), who used cadaver dissections to propose a kinematic model for human factors analysis, and Snyder et al. (15), who used cadaver dissection and radiographs of male volunteers in a variety of postures to obtain data on surface-landmark-to-skeleton transformations. The risks of radiography for healthy people have made such investigations unlikely to be performed today. Recently, Reynolds (16) conducted radiographic studies with a small number of human cadavers, but additional useful linkage data from healthy people in normal postures will probably have to be derived from MRI or other low-risk imaging techniques.

METHODS

KINEMATIC MODEL – The choice of the segments and joints for the kinematic model was based on an assessment of the needs for posture data in vehicle interior design. A vehicle occupant's posture can be represented in a number of ways, each of which has some advantages and disadvantages for use in vehicle design. In current SAE practice, the distribution of drivers' eye locations is predicted from vehicle geometry using statistical summaries of eye position data collected from a large number of people (3). The distribution of drivers' selected seat positions, which is closely related to their hip locations, is similarly predicted using a statistical summary of a large body of data (3). Both of these currently used models predict the spatial distribution of a single body landmark for an occupant population. The data on which they are based are, of course, the measured locations of these landmarks for a suitable population of drivers. Hence, one of the ways of representing vehicle occupant posture data is by statistical summaries of the locations of body landmarks for appropriately selected subjects. If these data are collected for a carefully selected range of vehicle interior geometries, then the resulting percentile accommodation models can accurately predict these landmark locations for a range of vehicles (4).

Recently, however, the use of three-dimensional software manikins to represent occupants in the vehicle design process has made more complete and integrated techniques necessary for representing occupant posture. To be useful in design, these manikins must not only represent appropriate combinations of anthropometric variables, but also must accurately represent the likely posture of an occupant with the specified body dimensions. Most currently available statistical summaries of driving posture, such as those represented by the SAE eye position (J941) and driver-selected seat position (J1517) practices, are severely limited for use in positioning CAD manikins, because they predict parameters of the population distribution of landmark locations, rather than the most likely landmark locations for a specific size of occupant. So, for example, the J941 eyellipse centroid represents a prediction of the average eye position for the U.S. population, but does not provide useful information about the most likely eye location for a person who is 1650 mm tall.

A primary emphasis in the current work is the representation of posture data in a way that can be readily interpreted to determine appropriate postures for CAD manikins of different sizes. There are many different ways of representing body posture, including body landmark locations, external body contours, and kinematic-linkage-model representations. While body landmark data are directly useful, particularly for prediction of eye and hip location, independent, simultaneous prediction of many individual landmark locations is inadequate for posturing CAD manikins, because the relative positions of the predicted landmark locations can be inconsistent with the

kinematic constraints imposed by the manikin's internal linkage. A method for interpreting postures in terms of a kinematic linkage is required.

Seidl (9) developed an innovative approach to representing posture using a kinematic linkage that is aligned using a person's external body contours in video images. The resulting posture analysis techniques were used to develop the RAMSIS software manikin, which is currently the only CAD manikin primarily intended for auto interior design that includes significant posture prediction capability. A limitation of the external contour fitting approach is that it does not generate external body landmark locations. Instead, the only representation of posture is in terms of the specific kinematic linkage used in the model. In the case of the RAMSIS model, the joints in the torso of the RAMSIS manikin are not intended to relate to specific anatomical joints, so the posture data from this approach cannot be readily generalized to other manikin linkages.

In the current work, a posture representation method has been developed that uses external body landmark locations to estimate the locations of joints that define the end points of body segments. The joints and segmentation scheme have been chosen because they provide the minimum complexity believed to be necessary to simulate the motions typical of changes between different vehicle occupant postures, while preserving an anatomical relationship between the external landmarks and the internal joints that define the linkage. This procedure is believed to allow findings reported using these techniques to be readily generalized to CAD manikins with a wide range of kinematic complexity. Using fewer segments would provide inadequate mobility, and using more segments, or using segments without explicit anatomical referents, would increase the difficulty in presenting and using posture data.

The kinematic model is depicted in Figures 1 and 2. The choice of the limb segments is straightforward. Individual hand, forearm, arm, thigh, leg, and foot segments are joined on each side of the body. In practice, the hand and forearm segments are considered as a single segment for representing normal riding and driving postures, since the complexities of hand movement relative to the arm are unimportant in that context. In the torso, the lumbar and cervical regions of the spine are each represented by a single segment and two joints. It appears from analysis of changes between different vehicle occupant postures that this approach represents sufficient kinematic complexity for representing normal riding and driving postures, and corresponds to the linkage most commonly used for dynamic crash victim simulation (10). The key determinant of model complexity for this application is that the linkage must adequately represent within-subject posture changes resulting from changes in vehicle layout and seat design within the rotational degrees-of-freedom of the linkage, i.e., without changing segment lengths. This is a necessary condition for interpreting the data using a limited-degree-of-freedom CAD manikin. For

example, eye-to-hip distance varies significantly with changes in lumbar support prominence (17). The selected linkage must allow this change in distance without violating the kinematic constraints. Analyses have demonstrated that the model presented here is kinematically adequate for representing normal driving postures (16).
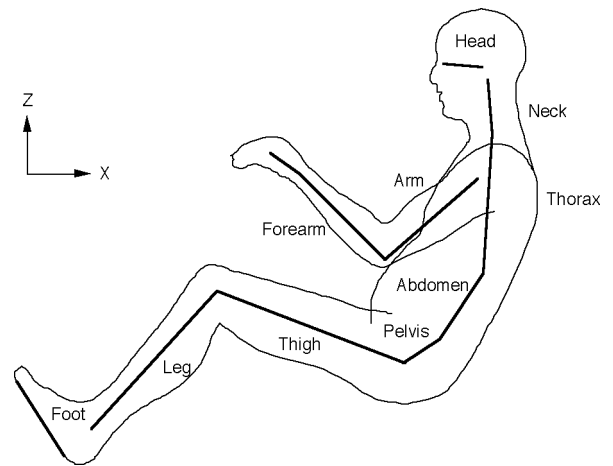

Figure 1. Kinematic model showing segments used to represent posture.

The joints in the model shown in Figure 2 correspond to approximate centers of rotation between adjacent bones and are located near the geometric center of particular anatomical joints. Some additional clarification of the nature of these joint locations may reduce potential confusion about their usage. The selected anatomical reference points correspond to joints in the kinematic model of human posture, and are generally located near the estimated anatomical center of a joint between bones, but are not necessarily at the actual center of rotation of the adjacent bones. As has been noted by many researchers, the instantaneous center of rotation between adjacent bones (or helical axis for three-dimensional rotation) changes position relative to the bones as the adjoining body parts are moved through their ranges of motion. This means that there is no single kinematic joint center at which all rotation between adjacent segments occurs.
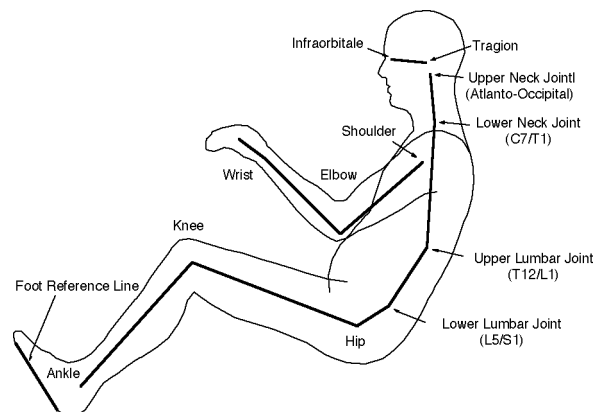

Figure 2. Joints in kinematic model used to represent vehicle occupant posture.

However, for representation of normal vehicle occupant posture, the range of motion of interest at each joint is usually small; that is, the range of postures associated with different seats and packages is small relative to the range of possible human postures, so the potential for movement of the kinematic joint centers relative to the body segments is also small. Where posture changes can be large, such as at the knee and elbow, the adjoining segments are long relative to the potential discrepancies between the actual and estimated joint centers, so kinematic errors associated with joint location estimates will also be small.

However, data represented using the techniques presented here may be applied to computer models that are used over much wider posture ranges, e.g., for reach assessments or ingress/egress studies. These models may rely on linkages that have joints located differently relative to the skeleton, or may have different linkages with more or fewer joints. Since the potential requirements of future models cannot be completely anticipated, the kinematic model joints in the current approach are anatomically defined, rather than kinematically defined. These joints are fixed in relation to skeletal landmarks and represent approximations of the center of rotation between adjacent bones. The relationships between these internal points (kinematic model joints) and external landmarks are thoroughly described in the following sections, so that the posture data reported using these techniques can be used in the future to estimate the location of any other bony reference point of interest, or to identify a joint location that is more suitable for a particular purpose. This approach is believed to provide a high level of generalizability for future modeling applications.

The orientation of the terminal segments (hands, feet, and head), are defined by vectors within the segments connecting landmarks of interest. Because the hands in normal driving and riding postures are, by definition, either on the steering wheel or resting on the thighs, the hand segment is assumed to be aligned with the forearm with whatever orientation (forearm pronation or supination) is appropriate to the task. For other occupant tasks, such as reaching, additional data on hand position and orientation could be collected.

An important distinction should be made between the use of this kinematic model for representing posture and for simulating posture changes. The model is used to represent posture when the posture is reported in terms of the lengths and orientations of the specified body segments. The corresponding posture can be reconstructed from this information and the model topology. Posture change for a particular subject can be represented by changes in orientation of model segments that were initially scaled to match the subject in a specific posture, or by a recalculation of each of the joint locations from new landmark data, resulting in different segment lengths and orientations. The latter approach has been used exclusively in this research for two reasons. The complexity of fitting a particular kinematic model to a new set of body landmark data is avoided, but, more importantly, the kinematic model has been found to be a sufficiently accurate representation of the human body linkage that the changes in apparent segment length between different sitting postures are small (18). Thus, the differences between the segment orientations obtained by fitting a single kinematic model to all of a particular subject's postures and those obtained by direct calculation of joint locations for each posture are also small.

For this approach to posture representation, the number of joint degrees of freedom are unimportant, because the lengths of segments are allowed to vary as needed. However, for simulations of posture changes using this model, the model segment lengths are fixed and articulated according to movement relationships developed from data. In simulations, the joint degrees of freedom are specified in the particular set of posture prediction functions that are used, which may vary depending on the application. Thus, for prediction of normal driving posture, the wrist may be assigned zero degrees of freedom, but for other tasks, two or more degrees-of-freedom may be simulated.

One substantial difference between the current kinematic model and other similar models is that the shoulder joint is not connected by a rigid link to the thorax. Instead, the position of the shoulder (glenohumeral) joint in a thorax-based coordinate system is reported. This allows the arm position resulting from complex motion of the clavicle and scapula to be described without reference to a mechanical linkage. This approach is believed to result in greater generality, particularly because the treatment of the shoulder complex varies widely among kinematic models of the body.

EXPERIMENTAL METHOD – A driver's posture is recorded by measuring the three-dimensional locations of body landmarks with respect to a vehicle coordinate system. The surface landmark locations are used to calculate the joint locations that define the kinematic model posture. These data may be obtained by many different techniques, including: photogrammetry of targets applied to the subject's skin or clothing, automated marker tracking systems, or by direct recording with three-dimensional coordinate measuring equipment, such as the FARO arm or SAC sonic digitizer. Each technique has advantages and disadvantages relating to accuracy, equipment cost, ease of use in vehicle and laboratory environments, and data processing requirements. In recent studies at UMTRI, landmark locations were measured using a Science Accessories Corporation GP8-3D sonic digitizer probe or a FARO Arm coordinate measurement device. Using both tools the experimenter first locates the landmark by direct palpation, then places the measuring probe at the landmark location to record the location. The pubic symphysis landmark is located by the subject. Each subject is trained to palpate down the midline of the abdomen until locating the symphysis. Assess-

ments of the precision of pelvis landmark measurements using these techniques suggest that they are sufficiently reliable for characterizing pelvis location and orientation (19).

BODY LANDMARKS – The experimenter palpated each landmark individually for each measurement to accurately locate the landmark and avoid the problems associated with movement of targets relative to the underlying bone. This technique also eliminated the need for target-to-landmark transformation calculations.

Table 1 and Figure 3 define and illustrate the body landmarks that are used to represent sitting posture with the kinematic model. These definitions are adapted from those in Schneider et al. (6), and are mostly identical or similar to those used in previous studies (15, 20). Note that some of these landmarks are not accessible when the subject is sitting in a vehicle seat. They can, however,

be collected when the subject is standing or sitting in a specially designed laboratory seat.

One important difference between these definitions and the conventional definitions is for the acromion landmark. In McConville et al. (20), the acromion landmark is defined as "the most lateral point on the lateral edge of the acromial process of the scapula." The definition used in Schneider et al. (6) is identical to McConville et al. This landmark definition is somewhat ambiguous because, on most subjects, the lateral margin of the acromion process extends for 10 to 20 mm in a sagittal plane, making a precise identification of the landmark in that plane difficult. For the current work, the definition of the acromion landmark has been refined to be the most anterior corner of the lateral margin of the acromion process. This bony point can be identified precisely on most subjects, and provides a more stable reference for shoulder location.

Table 1.   Definitions of Body Landmarks

Landmark	Definition
Glabella	Undepressed skin surface point obtained by palpating the most forward projection of the forehead in the midline at the level of the brow ridges.
Infraorbitale	Undepressed skin surface point obtained by palpating the most inferior margin of the eye orbit (eye socket).
Tragion	Undepressed skin surface point obtained by palpating the most anterior margin of the cartilaginous notch just superior to the tragus of the ear (located at the upper edge of the external auditory meatus).
Occiput	Undepressed skin surface point at the posterior inferior occipital prominence. Hair is lightly compressed.
Corner of Eye	Undepressed skin surface point at the lateral junction of the upper and lower eyelids.
C7, T8,* T12*	Depressed skin surface point at the most posterior aspect of the spinous process.
Suprasternale (manubrium)	Undepressed skin surface point at the superior margin of the jugular notch of the manubrium on the midline of the sternum.
Substernale (xyphoid process)	Undepressed skin surface point at the inferior margin of the sternum on the midline.
Anterior-Superior Iliac Spine (ASIS - right and left)	Depressed skin surface point at the anterior-superior iliac spine. Located by palpating proximally on the midline of the anterior thigh surface until the anterior prominence of the iliac spine is reached.
Posterior-Superior Iliac Spine* (PSIS - right and left)	Depressed skin surface point at the posterior-superior iliac spine. This landmark is located by palpating posteriorly along the margin of the iliac spine until the most posterior prominence is located, adjacent to the sacrum.
Pubic Symphysis	Depressed skin surface point at the anterior margin of pubic symphysis, located by the subject by palpating inferiorly on the midline of the abdomen until reaching the pubis. The subject is instructed to rock his or her fingers around the lower margin of the symphysis to locate the most anterior point.
Lateral Femoral Condyle	Undepressed skin surface point at the most lateral aspect of the lateral femoral condyle. Measured on the skin surface or through thin clothing.
Wrist	Undepressed skin surface point on the dorsal surface of the wrist midway between the radial and ulnar styloid processes.
Acromion	Undepressed skin surface point obtained by palpating the most anterior portion of the lateral margin of the acromial process of the scapula.
Lateral Humeral Condyle	Undepressed skin surface point at the most lateral aspect of the humeral condyle.
Lateral Malleolus	Undepressed skin surface point at the most lateral aspect of the malleolus of the fibula.
Medial Shoe Point	Point on the medial aspect of the right shoe medial to the first metatarsal-phalangeal joint (approximately the ball of the foot).
Shoe Heel Contact Point	Point on the floor at the center of the right shoe heel contact area with the foot in normal driving position contacting the accelerator pedal.

*These points are not accessible when the subject is sitting in a conventional vehicle seat, but are recorded in other sitting and standing experimental situations to characterize the subject's torso geometry. See text for details.
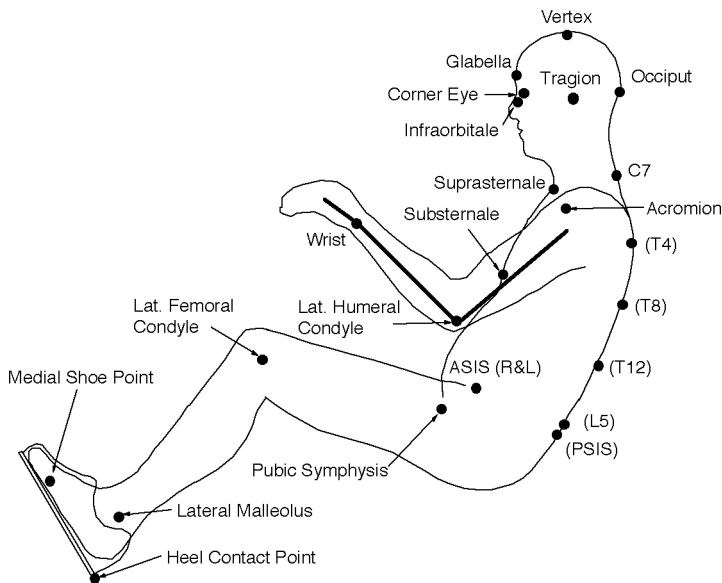
Figure 3. Body landmarks used to calculate internal joint locations and segment orientations.

The landmark set is sparse with regard to limb landmarks, reflecting the practical constraints of measuring vehicle occupant postures. Medial landmarks on the limbs are often difficult to reach with the measurement probes or to view with automated marker tracking systems, and the need to measure each subject in a large number of vehicle and seat conditions (in a typical study design) provides incentive to reduce the number of landmarks to shorten test times. However, because vehicle driving and riding postures are highly constrained, sufficient information to describe the posture is available with a sparse landmark set.

CALCULATION OF JOINT LOCATIONS – The kinematic model used to describe posture has joints that correspond to anatomical locations inside of the body. Calculation methods are needed to translate the exterior landmark locations to interior joint locations. This problem is common to any attempt to represent the body by a kinematic linkage, but is complicated because joint locations can be measured directly only with cadavers or through the use of x-rays or other internal imaging technology. Dempster (1) conducted the first large-scale effort to address this problem. He performed dissections of cadavers and made systematic measurements for the specific purpose of developing scalable linkage models of the human body for use in human factors analysis. Snyder et al. (15), in another important study, used radiography of male volunteers to study the locations and movements of the joints for a wide variety of seated and standing postures. Their specific emphasis was to determine the relationship between the motions of skin-mounted surface targets and the underlying joints.

Many researchers are currently performing biomechanical analysis of human activity using linkage models, and there are almost as many techniques for estimating internal joint locations from external, measurable locations of body landmarks to internal joints. In each case, the type of transformation chosen is dependent on the needs of the research. This section presents the calculation methods that have been selected based on the requirements of posture representation for automotive interior design using three-dimensional CAD manikins.

Data Sources – The landmark-to-joint transformation methods described here are based largely on the data and analysis presented by Schneider et al. (6) and Robbins (13, 14). This three-volume publication describes a detailed study of passenger-car drivers conducted to develop anthropometric specifications for crash-dummy design. Body landmark locations in a driving posture were recorded for 25 subjects in each of three size/gender groups: small females (approximately 5th-percentile U.S. by stature and weight), midsize males (approximately 50th-percentile U.S. by stature and weight), and large males (approximately 95th-percentile U.S. by stature and weight). The seated landmark data were supplemented by a large number of standard anthropometric measures and some developed specifically for automotive postures.

Robbins used the external landmark data to estimate internal joint locations, using skeleton geometry data from several sources. Table 2 shows the references for each of the model joints. In the current work, the original reference materials have been consulted to verify that the methods and estimates in Robbins (13) are valid. In the case of the upper lumbar and lower neck joints (T12/L1 and C7/T1), the data presented by Snyder et al. (15), on which Robbins relied, support a number of different location estimates, both because there is considerable variability in the data and because the data are presented in a number of different ways. A reexamination of the Snyder data indicated that the Robbins estimates were among the reasonable interpretations, so the location methods for these joints were selected to be consistent with Robbins. The only area in which the current methods differ substantially from Robbins is in the calculation of the hip and lower lumbar (L5/S1) joints. Robbins' analysis contains some discrepancies in regard to pelvis location that have been resolved by an analysis of data from several sources, including data from recent studies that were not available to Robbins.

Hip Joint Calculations – The location of the pelvis in the Robbins analysis has been criticized because of the large apparent flesh margin under the ischial tuberosities. Recent data from Reynolds (16) suggest that a typical flesh margin at the ischial tuberosities for a midsize-male cadaver on a rigid seat is about 16 mm, compared with about 42 mm in the Robbins analysis. The discrepancy appears to relate to the interpretation of the anterior-superior iliac spine (ASIS) landmarks relative to the ilia, which Robbins may have located too low on his pelvis reconstruction. Further, Robbins did not apparently include any flesh margin in the relationship between the measured ASIS location and the bone, which may have contributed to the discrepancy.

6

Because of these concerns about Robbins' estimates of the pelvis joint locations, the hip and lower lumbar joint (L5/S1) locations are estimated using pelvis landmark data with scaling methods developed from several other sources. Reynolds et al. (22) presented data on the positions of a large number of landmarks on pelves from a skeleton collection. Data were summarized for large male, midsize male, and small female pelves, categories selected so that the data would be applicable to the design of crash dummies of those sizes. Bell et al. (23) suggest using the distance between the anterior-superior iliac spine landmarks as a scaling dimension. A similar method was used by Manary et al. (24) in a study of driver hip joint locations. Recently, Seidel et al. (25) demonstrated that the use of other pelvis dimensions in addition to inter-ASIS breadth would improve the estimate of the hip joint center location. Data from each of these sources have been examined to determine the best method for calculating the hip joint locations.

Table 2.   Data Sources Used by Robbins (13) to Estimate Joint Locations

Joint	Reference	Type of Data
Upper Neck (atlanto-occipital)	Ewing and Thomas (21)	Kinematic analysis of head/neck motion
Lower Neck (C7/T1)	Snyder et al. (15)	Radiographic study of torso movement
Upper Lumbar (T12/L1)	Snyder et al. (15)	Radiographic study of torso movement
Wrist	Dempster (1)	Cadaver dissection
Elbow	Dempster (1)	Cadaver dissection
Knee	Dempster (1)	Cadaver dissection
Ankle	Dempster (1)	Cadaver dissection
Shoulder (glenohumeral)	Snyder et al. (15)	Radiographic study of torso movement

Seidel et al. (25) define three pelvis dimensions, illustrated in Figure 4: pelvis width (PW), which is the inter-ASIS distance; pelvis height (PH), which is the length of a line perpendicular to the inter-ASIS line to the pubic symphysis; and pelvis depth (PD), which is the distance from the ASIS to the posterior-superior iliac spine on the same side of the pelvis. They present the mean hip joint coordinates for 65 pelves relative to these dimensions. Table 3 compares the Seidel et al. scaling with that proposed by Bell et al. (23) from radiographic measurements, and that obtained from the Reynolds et al. (22) data. Figure 5 illustrates the X and Z coordinates. The Y coordinate is measured perpendicular to the midsagittal plane.

The scaling relative to pelvis width (inter-ASIS breadth) is very similar in the three studies, varying most in the X coordinate. There are larger discrepancies in the scaling based on pelvis height and pelvis depth. The four-percent difference between Seidel and Robbins in Hip-Z/PH pro-
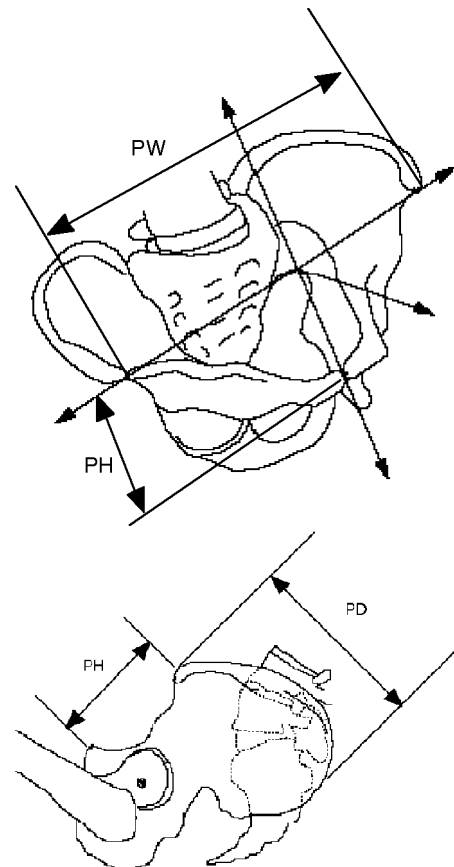
duces a difference in estimated hip joint location of about 3 mm for a midsize-male pelvis. The two-percent difference in Hip-X/PD also amounts to a difference of about 3 mm.

Seidel et al. found no statistically significant relationship between pelvis width and Hip-Z, suggesting that if pelvis width is the only available dimension, a constant value for Hip-Z, rather than the scaled value, could be used for all subjects. In contrast, Seidel et al. showed a significant relationship between Hip-Z and pelvis height, indicating that pelvis height would be a suitable scaling dimension for that coordinate. The improved performance of the pelvis-height scaling was demonstrated by a smaller mean estimation error (3.5 mm vs. 7.5 mm). Similarly, scaling Hip-X by pelvis depth produced a smaller mean error compared with scaling by pelvis width (3.0 mm vs. 4.9 mm). Notably, Seidel et al. also found no important differences between male and female pelves in these scaling relationships.

Figure 4.   Illustration of pelvis scaling dimensions: pelvis width (PW), pelvis height (PH), and pelvis depth (PD).

Table 3. Comparison of Hip Joint Location Methods: Mean Scaling Relationships

Measure*	Seidel et al. (24)	Bell et al. (23)	Reynolds et al. (22)†	Location Error Estimates** (mm)
Hip-X/PW	24%	22%	22%	4.9 (3.4)
Hip-Y/PW	36%	36%	37%	5.8 (4.2)
Hip-Z/PW	30%	30%	29%	7.5 (5.6)
Hip-X/PD	34%	--	32%	3.0 (2.3)
Hip-Z/PH	79%	--	83%	3.5 (2.8)

*The ratio of the coordinate value to the scaling dimension.
†Data from Reynolds et al. (22) are the averages of values for small-female, midsize-male, and large-male pelves.
** Mean (standard deviation) of prediction error from Seidel et al. (25), N = 65 except N = 35 for Hip-X/PD.
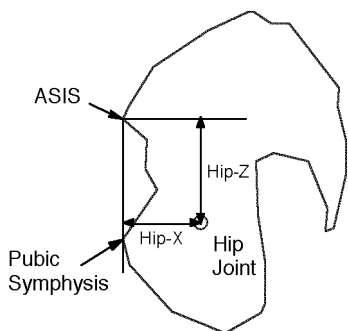

Figure 5. Location of the hip joint in the sagittal plane relative to the ASIS and pubic symphysis landmarks, showing the X and Z dimensions listed in Table 3.

The foregoing analysis led to the conclusion that the scaling relationships proposed by Seidel et al. should be used when the necessary data are available and reliable, meaning the locations of both ASIS, the pubic symphysis, and both PSIS landmarks. However, the Seidel et al. analysis demonstrated that the difference in error magnitudes for the alternative scaling techniques is small, so any of the techniques should give similar results.

Lower Lumbar Joint (L5/S1) Calculations – The joint between the fifth lumbar vertebra and first sacral vertebra can be considered to be a joint on the bony pelvis if motions within the sacral vertebrae and at the sacroiliac joints are assumed to be negligible. For analysis of seated postures, this is a reasonable assumption (26).

Reynolds et al. (22) include two data points on the top edge of the first sacral vertebra (S1) in the midsagittal plane. An offset vector of 10 mm, constructed perpendicular to the center of the line segment connecting the two S1 data points, was used to estimate the joint location, as shown in Figure 6.

The findings of Seidel et al. with respect to the superior scaling performance of pelvis height and pelvis depth for hip joint location suggest using those measures for estimating lower lumbar joint location as well. Table 4 shows

scaling percentages from Reynolds et al. for L5/S1 location estimated as described in Figure 6. Although there are differences between the small-female, midsize-male, and large-male pelves, they do not appear to be systematically related to body size. Given the lack of important gender differences in the Seidel et al. analysis, the mean scaling values from Robbins were selected.
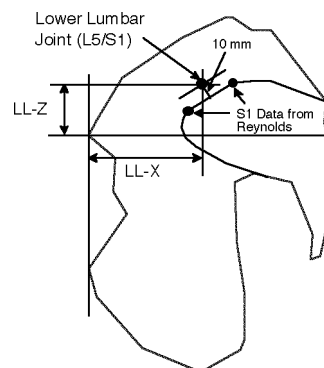

Figure 6. Method used to estimate lower lumbar joint (L5/S1) location from the data in Reynolds et al. (22). Not to scale.

Table 4. Scaling Relationships for L5/S1 from Reynolds et al. (22)

Measure	Small Female	Midsize Male	Large Male	Mean*
LL-X/PW	28.9%	26.4%	27.0%	27.4%
LL-Z/PW	17.2%	12.6%	15.1%	15.0%
LL-X/PD	42.5%	37.7%	39.4%	39.9%
LL-Z/PH	45.2%	39.9%	44.5%	43.2%

*Mean of small-female, midsize-male, and large-male values.

Flesh Margins – The preceding analyses of data relating to hip and lower lumbar joint location are based on landmarks on the pelvis bones. In live subjects, however, the landmark measurements are made through a thickness of compressed tissue. These flesh margin thicknesses are important to consider in calculating these joint locations. In previous analyses, Manary et al. (24) and others at UMTRI have used estimates of compressed flesh margin thickness of 5 mm at the ASIS and 15 mm at the pubic symphysis. Recently, a small-scale, unpublished study was conducted in which the flesh margins at these landmarks were measured directly in 30 male and female cadavers, using a probe configuration similar to that used to record body landmark data. Flesh margins of 10 mm at the ASIS and 15 mm at the pubic symphysis were found to be good estimates for all subjects. Accounting for clothing and differences between subject palpation and the cadaver experiments, flesh margins of 10 mm at the ASIS and 25 mm at the pubic symphysis are used.

Landmark Selection and Scaling for Other Joints – As with the pelvis joints, the locations of other joints relative to the surface landmarks are calculated using simple linear scaling relationships. Since Robbins presents a large set of surface landmark locations along with the joint

location estimates, it is possible to identify a number of different relationships among surface landmarks and joints that could be used to perform the transformations with new surface landmark data. The landmarks were selected to be as close as possible to those that were referenced in the original source materials listed in Table 2.

Since each joint lies some distance from the nearest measured landmark, a method must be developed to scale the vector relating the two, to account for differences in body size. In the current work, these joint location vectors are scaled by comparing the distance between two measured landmarks with the corresponding data for midsize males given by Robbins. This is analogous to the procedure used with pelvis landmarks. While the particular dimensions chosen may not be the ideal dimensions for scaling, they have been selected such that they are likely to be fairly well correlated with the vector magnitudes of interest. (In general, data on skeletal geometry necessary to test these assumptions are not available.) The scaling approach for all subjects uses the Robbins midsize-male data as the reference geometry because the underlying data on which the landmark-to-joint transformations are based (sources in Table 2) relied exclusively on male subjects. Table 5 lists the landmarks that define the location vectors and scaling measurements for each joint.

Table 5.   Landmarks Used To Define and Scale Joint Location Vectors

Joint	Landmarks
Upper Neck (atlanto-occipital)	Infraorbitale, Tragion
Lower Neck (C7/T1)	C7, Suprasternale
Upper Lumbar (T12/L1)	T8, T12, C7, Suprasternale
Lower Lumbar (L5/S1)	ASIS, PS, PSIS
Hip	ASIS, PS, PSIS
Shoulder	Acromion, C7, Suprasternale
Knee	Lateral Femoral Condyle (plus Hip Joint and Lateral Malleolus)
Elbow	Lateral Humeral Condyle (plus Shoulder Joint and Wrist landmark)
Wrist	Wrist
Ankle	Lateral Malleolus (plus Lateral Femoral Condyle and Hip Joint)

Shoulder Joint – The shoulder joint of the kinematic model approximates the anatomical glenohumeral joint, the articulation of the humerus with the glenoid fossa of the scapula. As noted above, the acromion landmark definition used here is slightly different than that used in other studies, resulting in a measurement point that is anterior to that measured using the more conventional definition. As a consequence, the acromion-to-shoulder-joint relationship in Robbins' data is different from the relationship in data measured using the current methods.

Robbins estimated the glenohumeral joint location by orienting a midsize-male humerus according to the measured humeral landmarks (greater tubercle, lateral epicondyle, and medial epicondyle). This procedure was used because the Dempster definition referred to an arm position dissimilar to a normal driving posture. Snyder et al. (15) report that the average sagittal-plane vector from the humeral head (approximately the glenohumeral joint center) to the acromion landmark is 52 mm long and oriented 42 degrees rearward from vertical, although there is considerable variability in both measurements. Starting from the glenohumeral joint location calculated by Robbins and applying the vector from Snyder et al. results in an estimated acromion location about 10 mm forward and 16 mm above the landmark location reported by Robbins. Alternatively, starting at the acromion location given by Robbins, the Snyder et al. vector predicts a humeral head location 16 mm below and 10 mm forward of that reported by Robbins. It should be noted that these discrepancies are within the range of the vector length data and vector angle data reported by Snyder et al.

The potential effects of the revised acromion definition were assessed by comparing the relative sagittal plane locations of suprasternale, C7, and acromion landmarks in data collected using the current definition and those reported by Robbins. Figure 7 shows mean values for 12 midsize males in one typical vehicle package from a recent UMTRI study, using the revised acromion definition, and those from Robbins for midsize males, aligned at C7 and rotated so that the C7-to-suprasternale vectors are at the same angle. The mean distance from C7 to suprasternale is 130 mm for the recent subjects and 138 mm for the Robbins subjects, indicating that the overall thorax size is similar. The acromion location reported by Robbins is considerably rearward and lower than the acromion location recorded using the revised landmark definition. The differences in the definitions may account for the more forward position, but no explanation is apparent for the vertical difference.

Since Robbins generated the glenohumeral joint location by using a humerus aligned with data from humeral landmarks, i.e., without relying on potentially lower-precision transformations from points on sternum or scapula, Robbins' joint location is assumed to be reasonably accurate. A transformation was developed to relate the revised acromion landmark to Robbins' glenohumeral joint location relative to C7 and suprasternale. Figure 7 shows that the glenohumeral joint location in the sagittal plane can be estimated by constructing a vector 58 mm long at an angle of 67 degrees with respect to the C7-to-suprasternale vector. The Snyder et al. data are difficult to interpret with regard to the necessity of scaling the acromion-to-humeral-head vector, because the data are not expressed in those terms. However, because it is reasonable to believe that the length of this vector will, on average, vary with body size, the length of the vector is scaled as a fraction of the C7-to-suprasternale vector, using the reference dimensions of 58 mm for acromion-to-glenohumeral-joint and 138 mm for C7-to-suprasternale, where the latter value is obtained from Robbins' midsize-male landmark data.
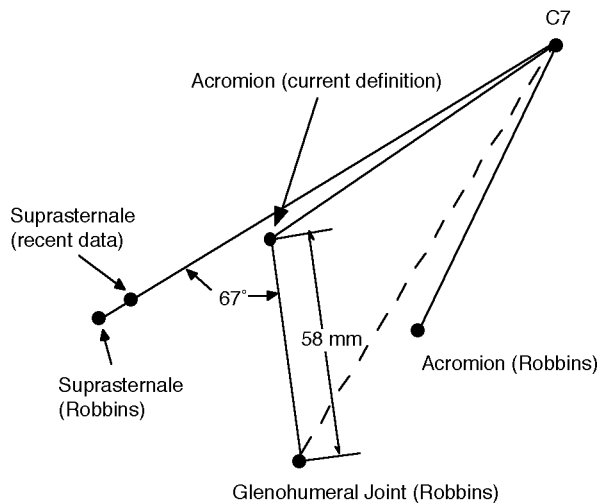
9

Figure 7. Acromion location comparison between current definition (N = 12 midsize males) and Robbins (N = 25 midsize males). Sideview data from Robbins have been aligned with the recent UMTRI data at C7 and rotated to align the C7-to-suprasternale vectors.

According to Snyder et al., the average angle from the center of the humeral head to the acromion landmark in the coronal (YZ) plane is only 2 degrees from vertical. Since the differences between the current and Snyder et al. acromion landmark definitions are believed to affect primarily the sagittal plane coordinates, the medial-lateral (Y-axis) coordinate of the shoulder (glenohumeral) joint will be taken to be the same as that of the acromion landmark.

This method for estimating the shoulder joint location for the kinematic model is based on fewer and less precise data than the methods for the hips and other extremity joints. However, the methods are likely to be sufficient for the intended applications.

Special Considerations for the Upper Lumbar Joint – The upper lumbar joint, which corresponds to the joint between the twelfth thoracic vertebra (T12) and the first lumbar vertebra (L1), is normally estimated, as indicated in Table 5, using the data from the T8 and T12 surface landmarks. However, these landmarks are not accessible when a subject is sitting in a normal automobile seat. Consequently, a method was developed to estimate the location of this joint from landmarks that are accessible in normal driving and riding postures.

Prior to posture measurement in the vehicle seat, the subject sits in a special laboratory seat that has approximately the same seatpan and seatback orientation as a normal vehicle seat, but has a 50-mm-wide slit in the center of the seatback that allows access to the spine. This seat is constructed with flat, rigid surfaces and is referred to as the "reference hardseat." With the subject sitting in the hardseat, the locations of suprasternale, C7, T8, and T12 are recorded. The data from T8 and T12 are used to calculate the location of the upper lumbar joint using the

scaling techniques described below. The data from C7 and suprasternale are also used to calculate the lower neck joint location (C7/T1). These two joints define the thorax segment for the subject. The length of the thorax segment (distance between the upper lumbar and lower neck joints) and the orientation of the vector between these joints relative to the C7-to-suprasternale vector is recorded for each subject. When analyzing subsequent test data from the subject in which T8 and T12 are not available, the location of the upper lumbar joint is calculated using the thorax geometry previously measured in the hardseat.

JOINT LOCATION DIAGRAMS – The Appendix contains complete information on the methods for calculating each joint in the kinematic model from the surface landmarks.

SUMMARY AND DISCUSSION

These procedures provide a means of representing a vehicle occupant's posture as a kinematic linkage, using joint locations calculated from a sparse set of external body landmarks. The joint location calculation procedures are based on a review of the literature, with particular emphasis on a recent study of driver anthropometry used to formulate anthropometric specifications for a new family of crash dummies. In all cases, the joint calculations are believed to be sufficiently accurate for representing normal vehicle occupant postures. Using these techniques, the effects of vehicle and seat design parameter as well as anthropometric factors on posture can be quantified and expressed in terms useful to the developers of ergonomic software.

ACKNOWLEDGEMENTS

REFERENCES

1. Dempster, W.T. (1955). *Space requirements of the seated operator: Geometrical, kinematic, and mechanical aspects of the body with special reference to the limbs.* WADC Technical Report 55-159. Wright-Patterson AFB, OH: Wright Air Development Center.

2. Nussbaum, M.A. and Chaffin, D.B. (1996). Development and evaluation of a scalable and deformable geometric model of the human torso. *Clinical Biomechanics* 11(1): 25-34.

3. Society of Automotive Engineers (1998). *Automotive Engineering Handbook*. Warrendale, PA: Society of Automotive Engineers, Inc.

4. Roe, R.W. (1993). Occupant packaging. In *Automotive Ergonomics*, ed. B. Peacock and W. Karwowski, 11-42. London: Taylor and Francis.

5. Backaitis, S.H., and Mertz, H.J., eds. (1994) *Hybrid III: The first human-like crash test dummy*. Special Publication PT-44. Warrendale, PA: Society of Automotive Engineers, Inc.

6. Schneider, L.W., Robbins, D.H., Pflüg, M.A., and Snyder, R.G. (1985). *Development of anthropometrically based design specifications for an advanced adult anthropomorphic dummy family, Volume 1*. Final report DOT-HS-806-715. Washington, DC: U.S. Department of Transportation, National Highway Traffic Safety Administration.

7. Schneider, L.W., Haffner, M.P., Eppinger, R.H., Salloum, M.J., Beebe, M.S., Rouhana, S.W., King, A.I., Hardy, W.N., and Neathery, R.F. (1992). Development of an advanced ATD thorax system for improved injury assessment in frontal crash environments. Technical Paper 922520. In *Proc. 36th Stapp Car Crash Conference*, pp. 129-155. Warrendale, PA: Society of Automotive Engineers, Inc.

8. Porter, J.M., Case, K., Freer, M.T., and Bonney, M.C. (1993). Computer-aided ergonomics design of automobiles. In *Automotive Ergonomics*, ed. B. Peacock and W. Karwowski, 43-77. London: Taylor and Francis.

9. Seidl, A. (1994). Das Menschmodell RAMSIS: Analyse, Synthese und Simulation dreidimensionaler Korperhaltungen des Menschen [The man-model RAMSIS: Analysis, synthesis, and simulation of three-dimensional human body postures]. Ph.D. dissertation, Technical University of Munich, Germany.

10. Maltha, J. and Wismans, J. (1980) MADYMO - Crash victim simulations, a computerised research and design tool. *Proc. 5th International IRCOBI Conference on the Biomechanics of Impact*, ed. J.P. Cotte and A. Charpenne, 1-13. Bron, France: IRCOBI.

11. Haas, W.A. (1989). Geometric model and spinal motions of the average male in seated postures. Master's thesis, Michigan State University, East Lansing.

12. Bush, N.J. (1993). Two-dimensional drafting template and three-dimensional computer model representing the average adult male in automotive seated postures. Master's thesis, Michigan State University, East Lansing.

13. Robbins, D.H. (1985a). *Anthropometric specifications for mid-sized male dummy, Volume 2*. Final report DOT-HS-806-716. Washington, DC: U.S. Department of Transportation, National Highway Traffic Safety Administration.

14. Robbins, D.H. (1985b). *Anthropometric specifications for small female and large male dummies, Volume 3*. Final report DOT-HS-806-717. Washington, DC: U.S. Department of Transportation, National Highway Traffic Safety Administration.

15. Snyder, R.G., Chaffin, D.B., and Schutz, R. (1972). *Link system of the human torso.* Report no. AMRL-TR-71-88. Wright-Patterson Air Force Base, OH: Aerospace Medical Research Laboratory.

16. Reynolds, H.M. (1994). *Erect, neutral, and slump sitting postures: A study of the torso linkage system from shoulder to hip joint.* Final Report AL/CF-TR-1994-0151. Wright Patterson Air Force Base, OH: Air Force Material Command.

17. Reed, M.P. and Schneider, L.W. (1996). Lumbar support in auto seats: Conclusions from a study of preferred driving posture. Technical Paper No. 960478. In *Automotive Design Advancements in Human Factors (SP-1155),* pp. 19-28. Society of Automotive Engineers, Warrendale, PA.

18. Reed, M.P. (1998). Statistical and Biomechanical Prediction of Automobile Driving Posture. Doctoral Dissertation. University of Michigan, Ann Arbor, MI.

19. Reed, M.P., Schneider, L.W., and Eby, B.A.H. (1995). *The effects of lumbar support prominence and vertical adjustability on driver postures*. Technical Report UMTRI-95-12. Ann Arbor: University of Michigan Transportation Research Institute.

20. McConville, J.T., Churchill, T.D., Kaleps, I., Clauser, C.E., and Cuzzi, K. (1980). *Anthropometric relationships of body and body segment moments of inertia.* Report no. AMRL-TR-80-119. Wright Patterson Air Force Base, OH: Aerospace Medical Research Laboratories.

21. Ewing, C.L., and Thomas D.J. (1972) *Human head and neck response to impact acceleration.* NAMRL Monograph 21. Pensacola, FL: Naval Aerospace Medical Research Laboratory.

22. Reynolds, H.M., Snow, C.C., and Young, J.W. (1981). *Spatial Geometry of the Human Pelvis.* Memorandum Report AAC-119-81-5. Oklahoma City, OK: Federal Aviation Administration, Civil Aeromedical Institute.

23. Bell, A.L., Pedersen, D.R., and Brand, R.A. (1990). A comparison of the accuracy of several hip center location prediction methods. *Journal of Biomechanics* 23(6): 617-621.

24. Manary, M.A., Schneider, L.W., Flannagan, C.C., and Eby, B.H. (1994). Evaluation of the SAE J826 3-D manikin measures of driver positioning and posture. Technical Paper 941048. Warrendale, PA: Society of Automotive Engineers, Inc.

25. Seidel, G.K., Marchinda, D.M., Dijkers, M., and Soutas-Little, R.W. (1995). Hip joint center location from palpable bony landmarks--A cadaver study. *Journal of Biomechanics* 28(8): 995-998.

26. Andersson, G.B.J., Murphy, R.W., Örtengren, R., and Nachemson, A.L. (1979). The influence of backrest inclination and lumbar support on lumbar lordosis. *Spine* 4(1), 52-58.

APPENDIX

CALCULATION DIAGRAMS FOR ALL JOINTS

This section contains detailed descriptions of the calculation procedures for each joint, along with figures depicting the scaling methods. As noted above, torso postures are restricted to being sagittally symmetric. Consequently, torso joint locations are calculated in the midsagittal XZ plane only, which is assumed to be parallel to the vehicle or seat XZ (sideview) plane. Extremity joints are located in three dimensions.

These landmark-to-joint transformations are presented in terms of rotated and scaled vectors. They could instead be presented in terms of segment-specific coordinate systems, but the current, equivalent procedure was judged to be simpler to present and closer to the manner in which such transformations would be implemented in computer software.

UPPER NECK JOINT – The upper neck joint corresponds anatomically to the atlanto-occipital joint. Figure 8 shows the technique for calculating the location of the upper neck joint from the infraorbitale and tragion landmarks, measured on the same side of the body. In the XZ plane, the upper neck joint center is located by rotating a vector from tragion to infraorbitale downward through 117 degrees. The vector length is 31 percent of the measured sagittal plane distance from tragion to infraorbitale. If a Y coordinate for the upper neck joint is required, it can be estimated by using the Y-coordinate of the mid-tragion or mid-infraorbitale point, i.e., centerline of head.
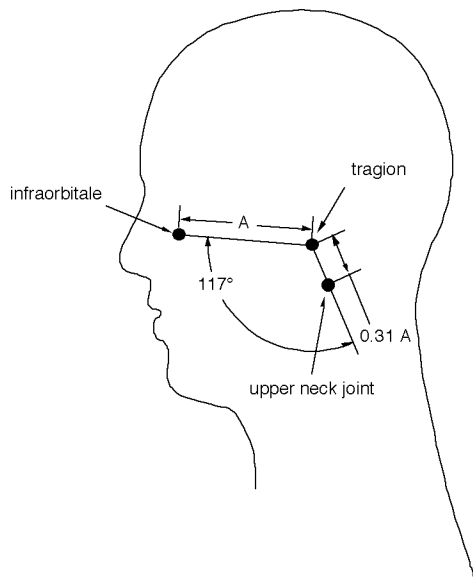

Figure 8.   Calculation techniques for upper neck joint.

LOWER NECK JOINT – The lower neck joint corresponds anatomically to the C7/T1 joint. The location of this joint is calculated using the C7 and suprasternale surface landmarks, as shown in Figure 9. The vector

from C7 to suprasternale is rotated upward 8 degrees and scaled to have a length equal to 55 percent of the measured sagittal-plane distance from C7 to suprasternale.

UPPER LUMBAR JOINT – The upper lumbar joint corresponds anatomically to the T12/L1 joint. With the subject sitting in the reference hardseat, the locations of suprasternale, C7, T8, and T12 are recorded. The data from T8 and T12 are used to calculate the location of the upper lumbar joint, as shown in Figure 9.
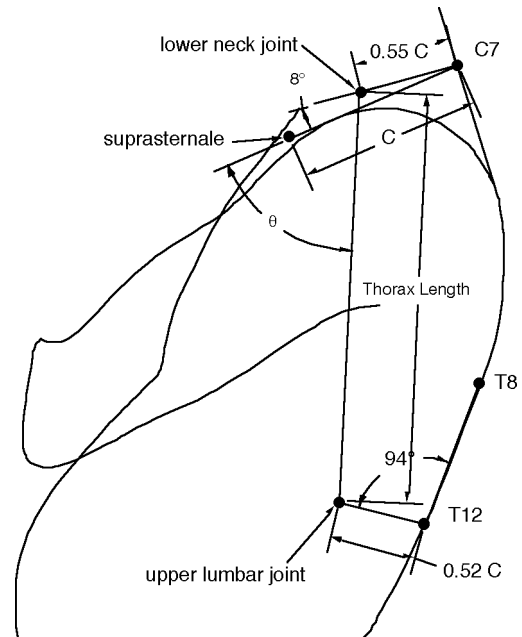

Figure 9.   Calculation method for lower neck joint and upper lumbar joint.

Suprasternale and C7 data are used to calculate the lower neck joint location as described above. The thorax length (the distance from the lower neck joint to the upper lumbar joint) and the angle θ (formed by the thorax segment and the C7-to-suprasternale vectors) are recorded for the subject using data collected in the reference hardseat (see above). These two values comprise the subject's thorax geometry for subsequent posture calculations.

When the subject's posture is measured in experimental vehicle conditions, the locations of suprasternale and C7 are used to calculate the lower neck joint location as described above. A thorax segment vector is then constructed and oriented relative to the C7-to-suprasternale vector based on the subject's thorax geometry obtained in the hardseat.

SHOULDER JOINT – The shoulder joint calculation in the sagittal plane is shown in Figure 10. The sagittal-plane distance from the shoulder joint to acromion landmark is 42 percent of the distance from C7 to suprasternale on a vector forming an angle of 67 degrees with the C7 to suprasternale vector. The Y-axis (medial-lateral)

position of the shoulder joint is taken to be the same as the Y coordinate of the acromion landmark. Since the postures are restricted to sagittal symmetry, the contralateral shoulder joint has the same X and Z coordinate, and lies the same distance lateral from the C7 landmark.
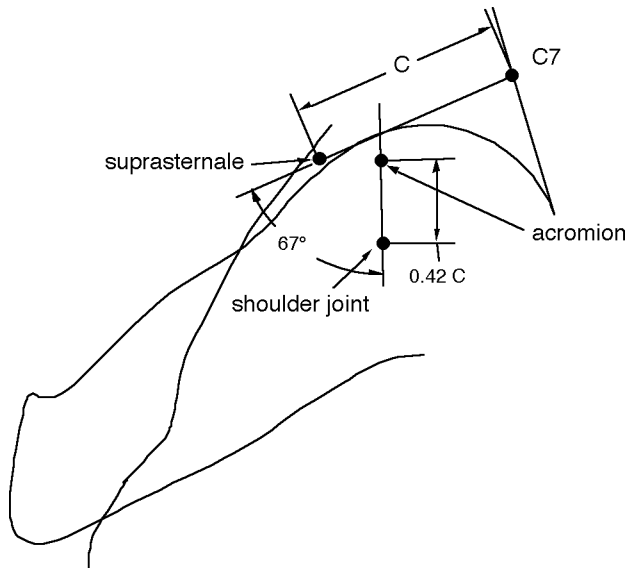

Figure 10. Calculation method for the shoulder joint.

LOWER LUMBAR JOINT AND HIP JOINTS – The hip joint and lower lumbar joint locations are calculated using the anterior-superior iliac spine (ASIS) landmarks (right and left), the pubic symphysis (PS) landmark, and the posterior-superior iliac spine landmark (PSIS). Calculations are conducted in three dimensions to obtain good estimates of both the left and right hip joint center locations for subsequent calculation of lower extremity posture. Although the measured postures are nominally sagittally symmetric and aligned with the package axes, a test subject's pelvis is sometimes tilted laterally or twisted relative to the package coordinate system. Consequently, the hip joint locations are calculated individually, then averaged in the XZ plane to obtain a mean hip joint location for use in calculating pelvis segment orientation (pelvis angle).

The lower lumbar and hip joint locations are calculated in a pelvis-centered coordinate system, which is then transformed to the desired global coordinate system. The pelvis coordinate system is shown in Figure 11. The Y axis is defined by the vector connecting the left and right ASIS. The Z axis is perpendicular to this line and passes through the pubic symphysis (PS). The X axis is mutually perpendicular to the Y and Z axes. Note that the coordinate system shown in Figure 11 is based on points on the bone, rather than surface landmarks. The flesh margins at the ASIS and PS landmarks are taken into account in the calculations.
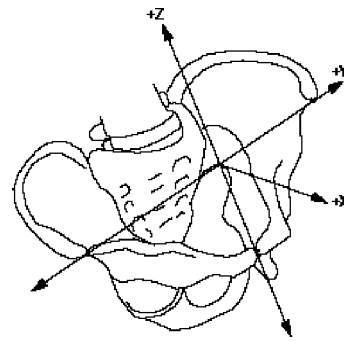

Figure 11. Pelvis coordinate system, adapted from Reynolds et al. (22).

The first step in the calculation of pelvis joints is to account for flesh margins at the landmarks. Using the rationale described above, margins of 10 mm at the ASIS and 25 mm at the pubic symphysis are used. A landmark-to-bone margin of 10 mm at the PSIS is used. As shown in Figure 12, a preliminary surface pelvis coordinate system {Xs, Ys, Zs} is established using the definition in Figure 11 with the ASIS and PS surface landmarks. The landmark points are then translated according to the flesh margins to obtain estimates of the underlying bony landmark location. The bone points are then used to define a pelvis bone coordinate system {Xb, Yb, Zb} identical to that shown in Figure 11. Table 6 shows the flesh margin correction vectors in the surface pelvis coordinate system.
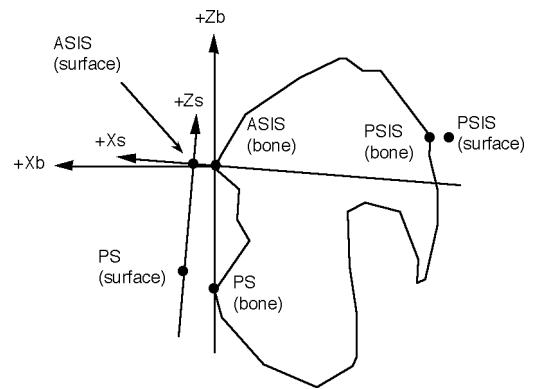

Figure 12. A sagittal view of surface and bone pelvis coordinate systems based on measured landmark locations (not to scale).

Table 6. Flesh Margin Correction Vectors in the Surface Pelvis Coordinate System {Xs, Ys, Zs} (mm)

Landmark	X	Y	Z
ASIS (right and left)	-10	0	0
PS	-17.7	0	-17.7
PSIS	5	0	0

13

The locations of the hip and lower lumbar (L5/S1) joints are calculated in the bone coordinate system $\{X_b, Y_b, Z_b\}$ using vectors scaled with reference to pelvis dimensions defined by the bone landmark locations. The reference dimensions, all measured in three dimensions, are as follows:

Pelvis Width (PW): Distance between right ASIS (bone) and left ASIS (bone).

Pelvis Height (PH): Distance between PS (bone) and the midpoint of the line connecting left ASIS (bone) and right ASIS (bone).

Pelvis Depth (PD): Distance between right ASIS (bone) and right PSIS (bone) or the distance between left ASIS (bone) and left PSIS (bone); if all four landmarks are available, use average of values from left and right sides.

Figure 13 shows the X and Z coordinates of the hip and lower lumbar joints. Tables 7 and 8 give the scaling relationships to be used. Note that the X and Z coordinates may be scaled using PW or PD and PH, respectively. The latter should be used when the required landmark data are available. The Y coordinate of the lower lumbar joint in the bone coordinate system is zero, i.e., equal to the Y coordinate of the midpoint of the line connecting right ASIS (bone) and left ASIS (bone). The Y coordinate of the hip joints are found by moving laterally right or left from the mid-ASIS point according to the scaling in Table 7.
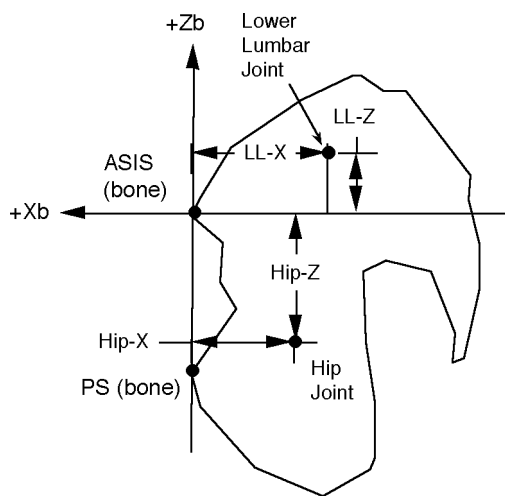

Figure 13. Location of hip and lower lumbar joints in XZ plane relative to bone coordinate system (not to scale). See Tables 7 and 8 for dimension scaling.

Table 7. Mean Hip Joint Scaling Relationships from Seidel et al. (25)

Measure*	Scale Factor
Hip-X/PW	24%
Hip-Y/PW	36%*
Hip-Z/PW	30%

*Y coordinate measured laterally from the mid-ASIS point.

Table 7. Mean Hip Joint Scaling Relationships from Seidel et al. (25)

Measure*	Scale Factor
Hip-X/PD	34%
Hip-Z/PH	79%

*Y coordinate measured laterally from the mid-ASIS point.

Table 8. Mean Lower Lumbar Joint Scaling Relationships Using Data from Reynolds et al. (22)

Measure*	Scale Factor
LL-X/PW	27.4%
LL-Z/PW	15.0%
LL-X/PD	39.9%
LL-Z/PH	43.2%

LOWER EXTREMITY – The knee and ankle joint locations are calculated using simplifications of the techniques described by Dempster (1) and adapted by Robbins (13). Both the Dempster and Robbins procedures locate these joints on vectors connecting landmarks on opposite sides of the limb. Because it is often difficult to measure the locations of medial landmarks with vehicle-seated occupants, the simplified procedures use data from only the lateral side of the limb to obtain reasonably similar results. The procedure is to project a vector a scaled distance perpendicular to the plane formed by two measured and one calculated landmark. The scaling was developed from data on limb breadth at the joints in Schneider et al. (6). Figure 14 shows the procedure schematically.

To calculate the knee joint location, a plane is formed by the measured lateral malleolus and lateral femoral condyle locations, along with the calculated hip joint location on the same side of the body. A vector is constructed perpendicular to this plane, passing through the lateral femoral condyle landmark. The knee joint is located on this vector medial to the lateral femoral condyle landmark by a distance equal to 11.8 percent of the measured distance between the lateral malleolus and the lateral femoral condyle landmarks.

The ankle joint location is calculated similarly. A vector is constructed perpendicular to the plane described above, and passing through the lateral malleolus landmark. The ankle joint is located medial to the lateral malleolus landmark by a distance equal to 8.5 percent of the distance between the lateral malleolus and the lateral femoral condyle landmarks.
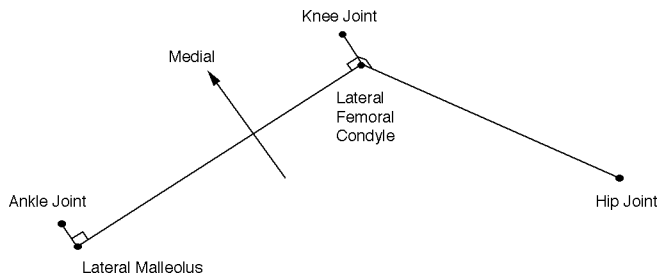
Figure 14. Calculation procedure for knee and ankle joints. Vectors from knee joint to lateral femoral condyle, and from ankle joint to lateral malleolus, are perpendicular to the plane formed by the hip joint, lateral femoral condyle, and lateral malleolus. See text for scaling length of vector from lateral femoral condyle to knee joint.

UPPER EXTREMITY – Calculations of upper extremity joint locations are similar to those for the lower extremity. Because of pronation and supination of the forearm, more than one wrist landmark would be necessary to use a method similar to the ankle technique to locate the wrist joint. However, a single point on the dorsal surface of the wrist is a sufficiently accurate estimate of the joint location for representing normal riding and driving postures. The measured wrist point is a skin surface point midway between the palpated radial and ulnar styloid processes.

The elbow location is calculated in a manner analogous to the knee, as shown in Figure 15. A plane is constructed that passes through the wrist landmark, lateral humeral condyle landmark, and the shoulder joint location on the same side of the body. A vector is constructed perpendicular to this plane, passing through the lateral humeral condyle landmark. The elbow joint is located medial to the lateral humeral condyle landmark a distance equal to 15.5 percent of the distance between the lateral humeral condyle and wrist landmarks. This scaling was determined from data on elbow width as a percentage of forearm length in Schneider et al. (6).
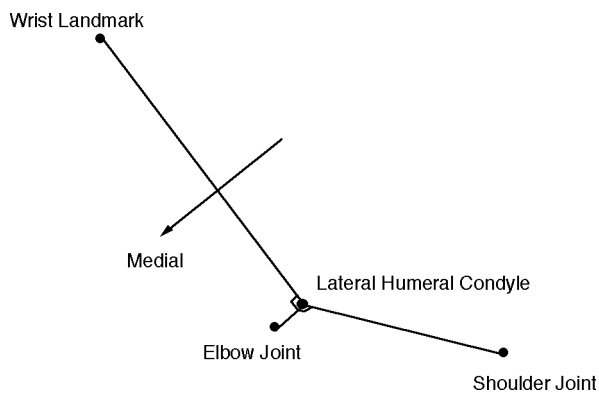

Figure 15. Calculation procedure for elbow joint. Vector from lateral humeral epicondyle to elbow joint is perpendicular to plane formed by the shoulder joint, lateral humeral epicondyle, and wrist landmark.